

Supplementary materials

Identifying the mechanisms by which irrigation can cool urban green spaces in summer

Pui Kwan Cheung^a, Naika Meili^{b,c}, Kerry A. Nice^d, Stephen J. Livesley^a

^aSchool of Agriculture, Food and Ecosystem Sciences, Burnley Campus, University of Melbourne, 500 Yarra Boulevard, Richmond, VIC 3121, Australia

^bDepartment of Civil and Environmental Engineering, National University of Singapore, Singapore, Singapore

^cFuture Cities Laboratory Global, Singapore-ETH Centre, Singapore, Singapore

^dTransport, Health, and Urban Systems Research Lab, Faculty of Architecture, Building, and Planning, the University of Melbourne, Parkville, VIC 3010, Australia

Corresponding author: Pui Kwan Cheung (cheung.p@unimelb.edu.au)

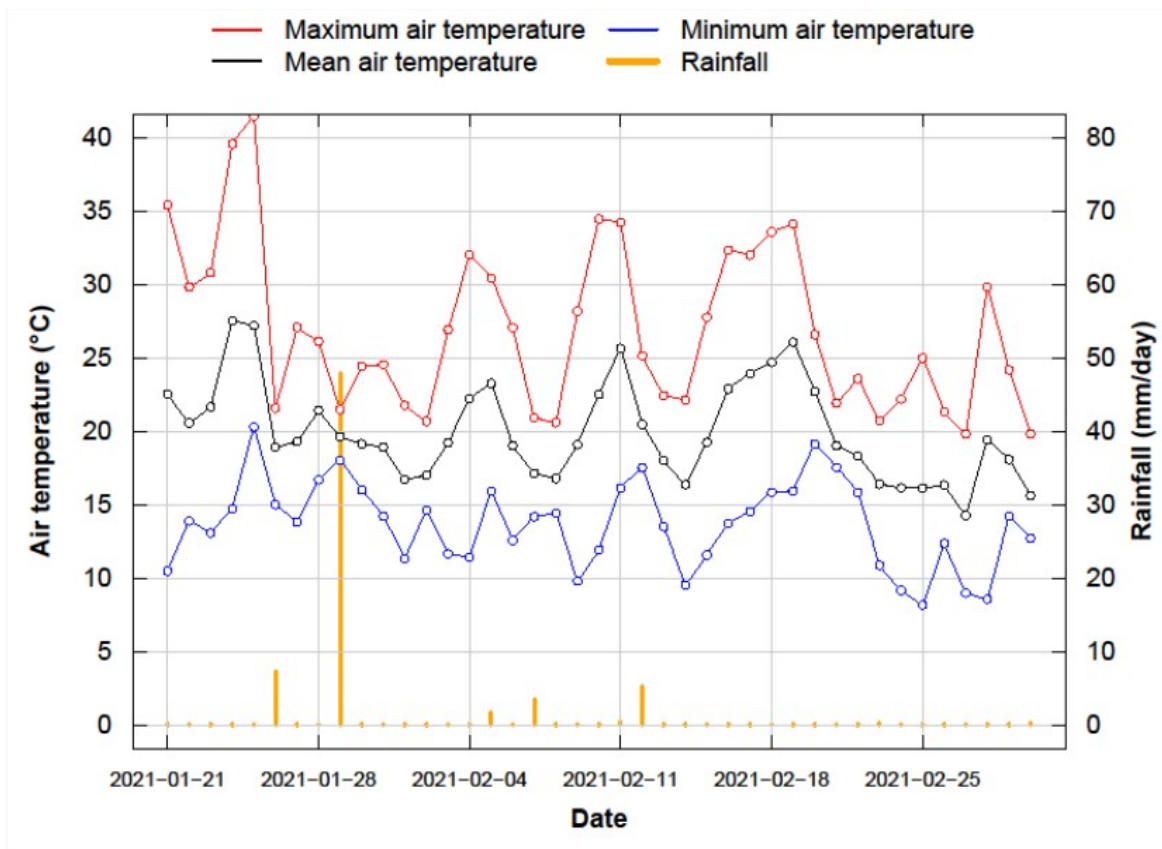


Fig. S1. Daily minimum, mean and maximum air temperatures and total rainfall of the model testing period (2021-01-21 to 2021-03-02, 41 days).

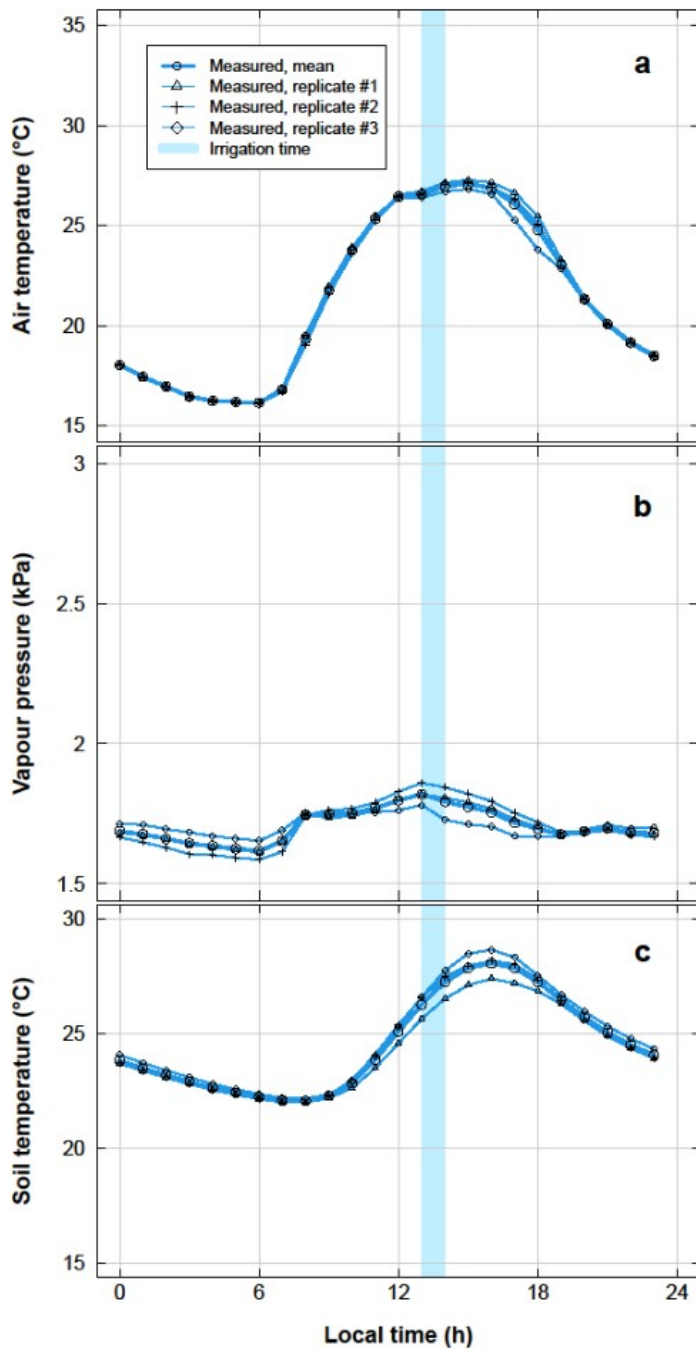


Fig. S2. The average diurnal cycle of measured (a) air temperature, (b) vapour pressure, and (c) soil temperature of the three replicated plots with irrigation. The measurement period was from 2022-01-28 to 2022-03-06 (38 days).

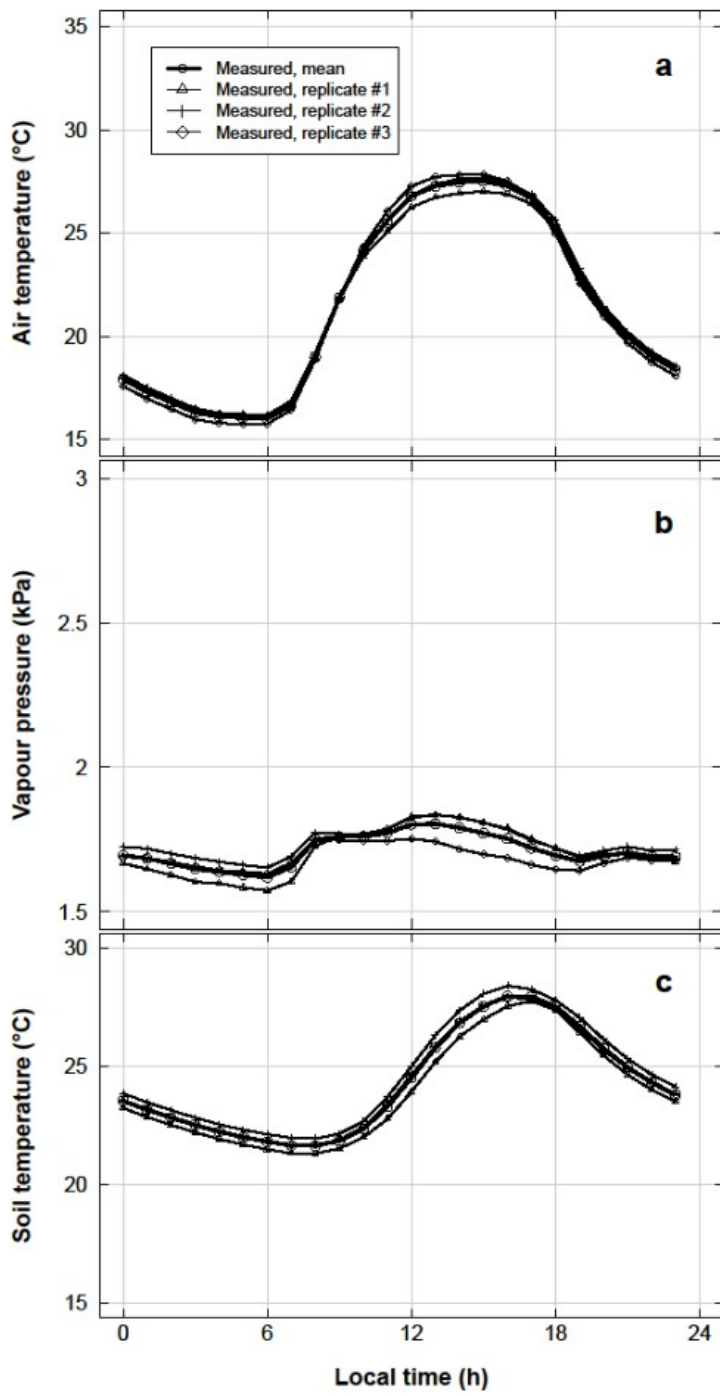


Fig. S3. The average diurnal cycle of measured (a) air temperature, (b) vapour pressure, and (c) soil temperature of the three replicated plots without irrigation. The measurement period was from 2022-01-28 to 2022-03-06 (38 days).

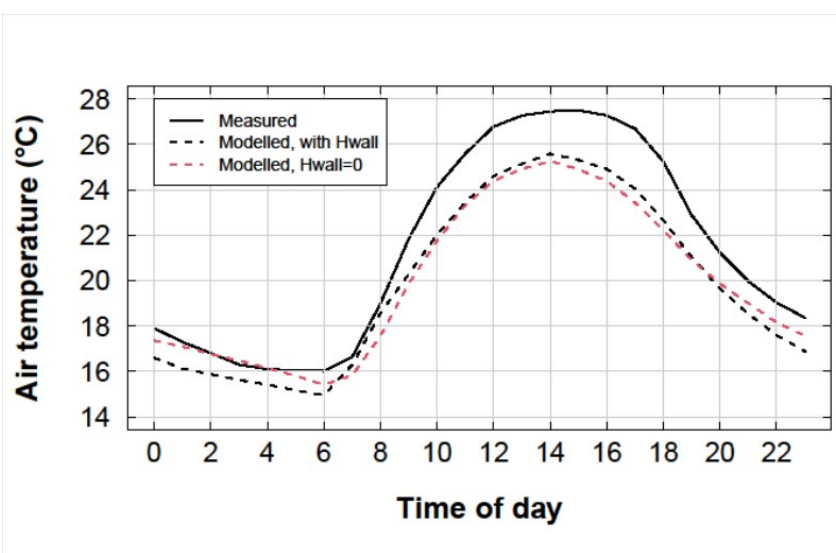


Fig. S4. Comparing measured 2-m air temperature to modelled 2-m air temperature with and without the sensible heat flux from the building walls (H_{wall}) in the average diurnal cycle of the unirrigated case in the model evaluation period (2022-01-28 to 2022-03-06). The presence or absence of sensible heat from canyon building walls had little impact on modelled air temperature, particularly during the day.

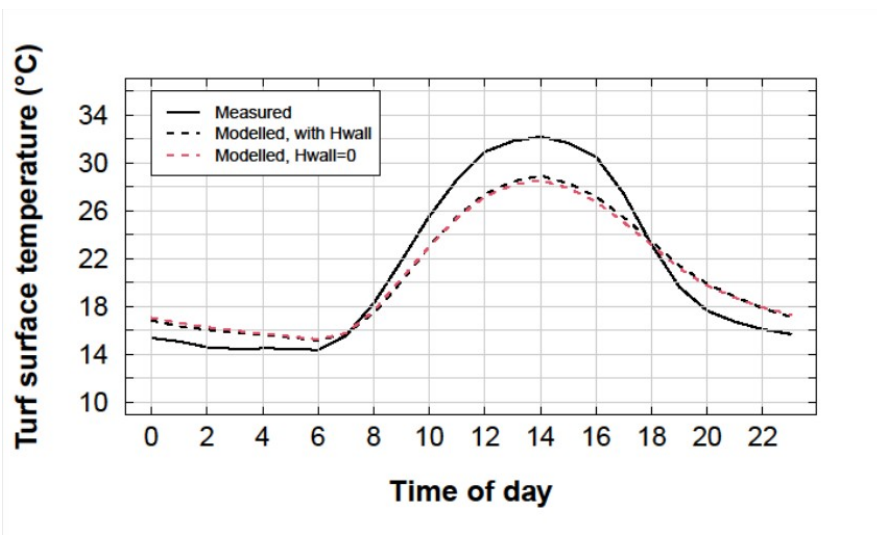


Fig. S5. Comparing measured turf surface temperature to modelled turf surface temperature with and without the sensible heat flux from the building walls (H_{wall}) in the average diurnal cycle of the unirrigated case in the model evaluation period (2022-01-28 to 2022-03-06). The presence or absence of sensible heat from canyon building walls had little impact on modelled turf surface temperature.

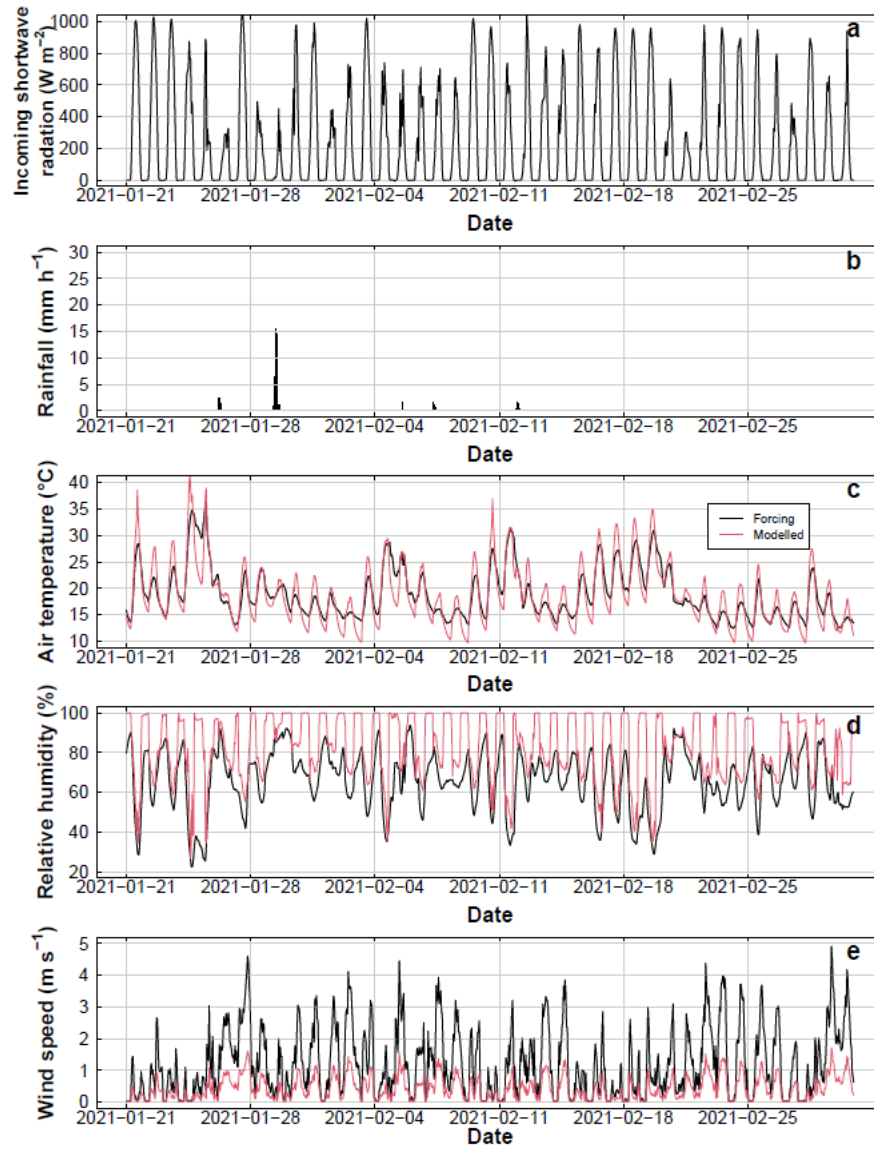


Fig. S6. Forcing data of the model testing period: (a) incoming shortwave radiation, (b) rainfall, (c) air temperature, (d) relative humidity, and (e) wind speed. The modelled results (2 m above ground) for air temperature, relative humidity and wind speed are also included.

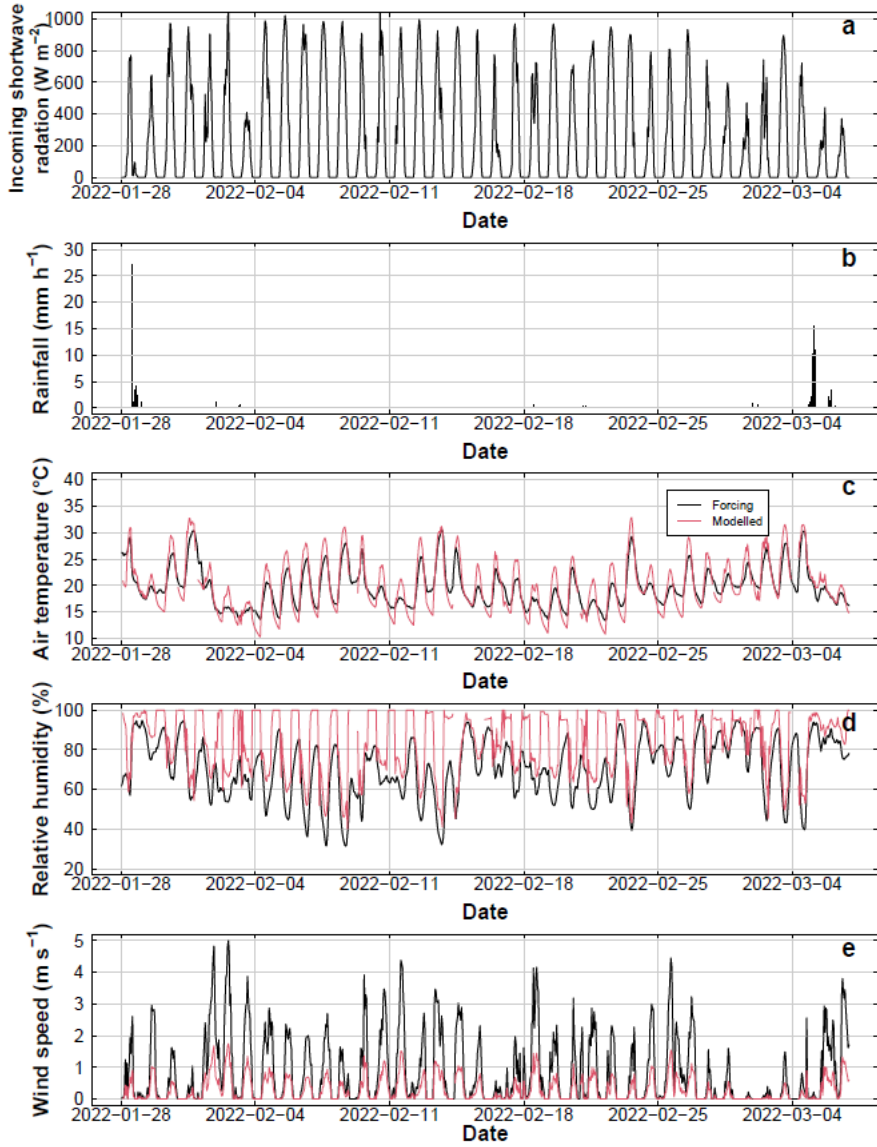


Fig. S7. Forcing data of the model evaluation period: (a) incoming shortwave radiation, (b) rainfall, (c) air temperature, (d) relative humidity, and (e) wind speed. The modelled results (2 m above ground) for air temperature, relative humidity and wind speed are also included.

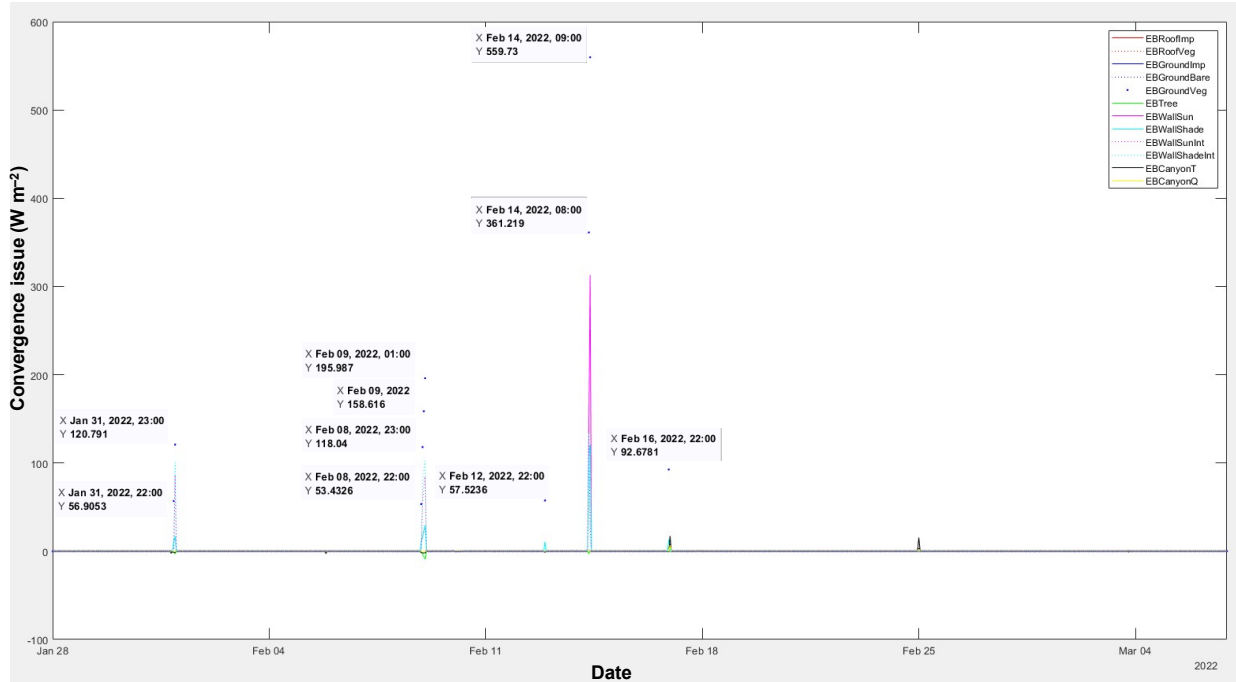


Fig. S8. Convergence issues of the unirrigated scenario. The energy balance of ground vegetated surface (EBGroundVeg) failed to converge in a number of time steps in the simulation. Those time steps were removed from the analysis.

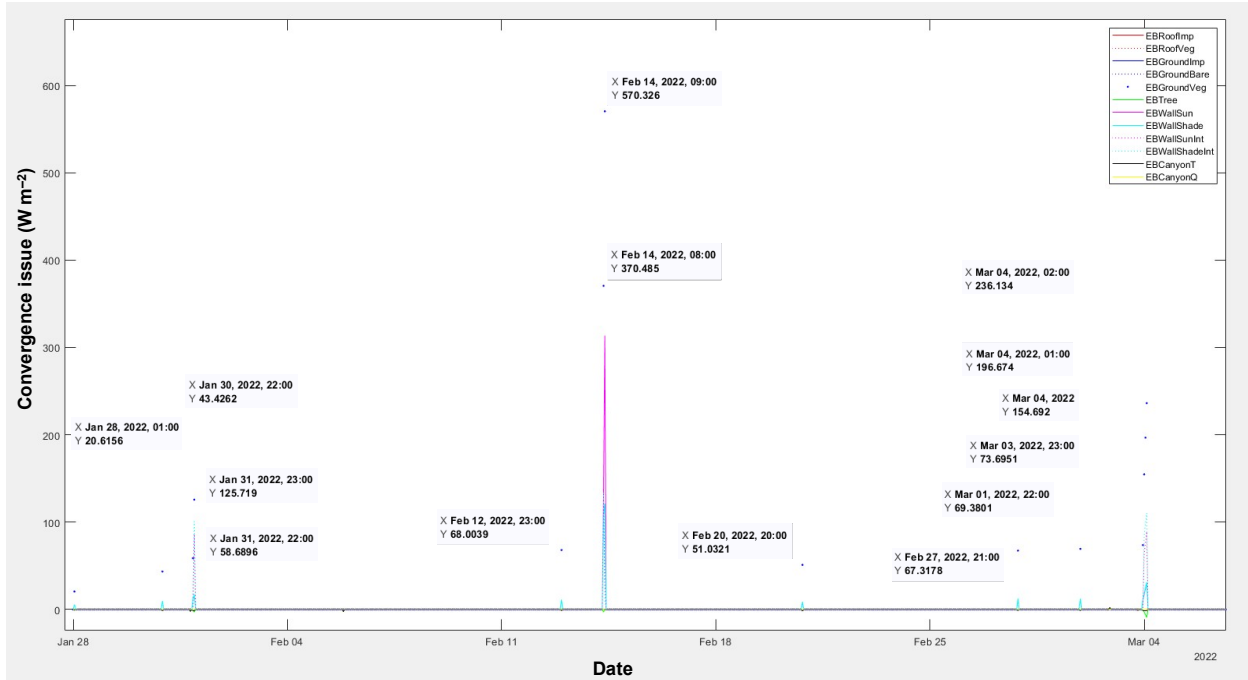


Fig. S9. Convergence issues of the irrigated scenario. The energy balance of ground vegetated surface (EBGroundVeg) failed to converge in a number of time steps in the simulation. Those time steps were removed from the analysis.

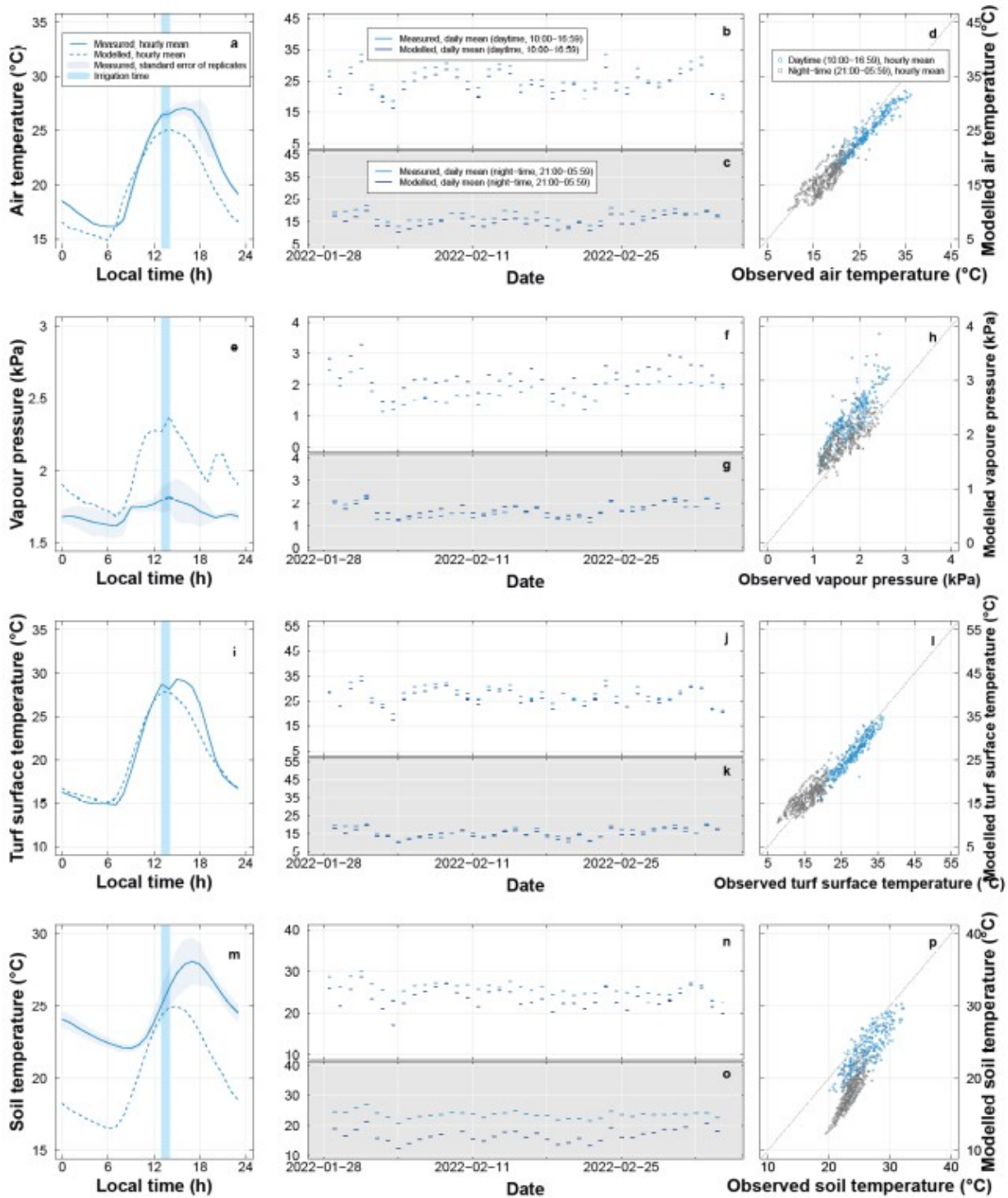


Fig. S10. Model evaluation that compared the modelled and the measured (a–d) air temperature, (e–h) vapour pressure (i–l) turf surface temperature, (m–p) soil temperature of the irrigated scenario (plot). The modelled and measured data were compared in terms of their average diurnal cycles (left column),

daytime and night-time daily means (middle column) and scatter plot of hourly means (right column). In the middle column, the broken lines were a time series split into daytime (10:00–16:59, white panels) and night-time (21:00–05:59, grey panels). The model evaluation period was from 2022-01-28 to 2022-03-06.

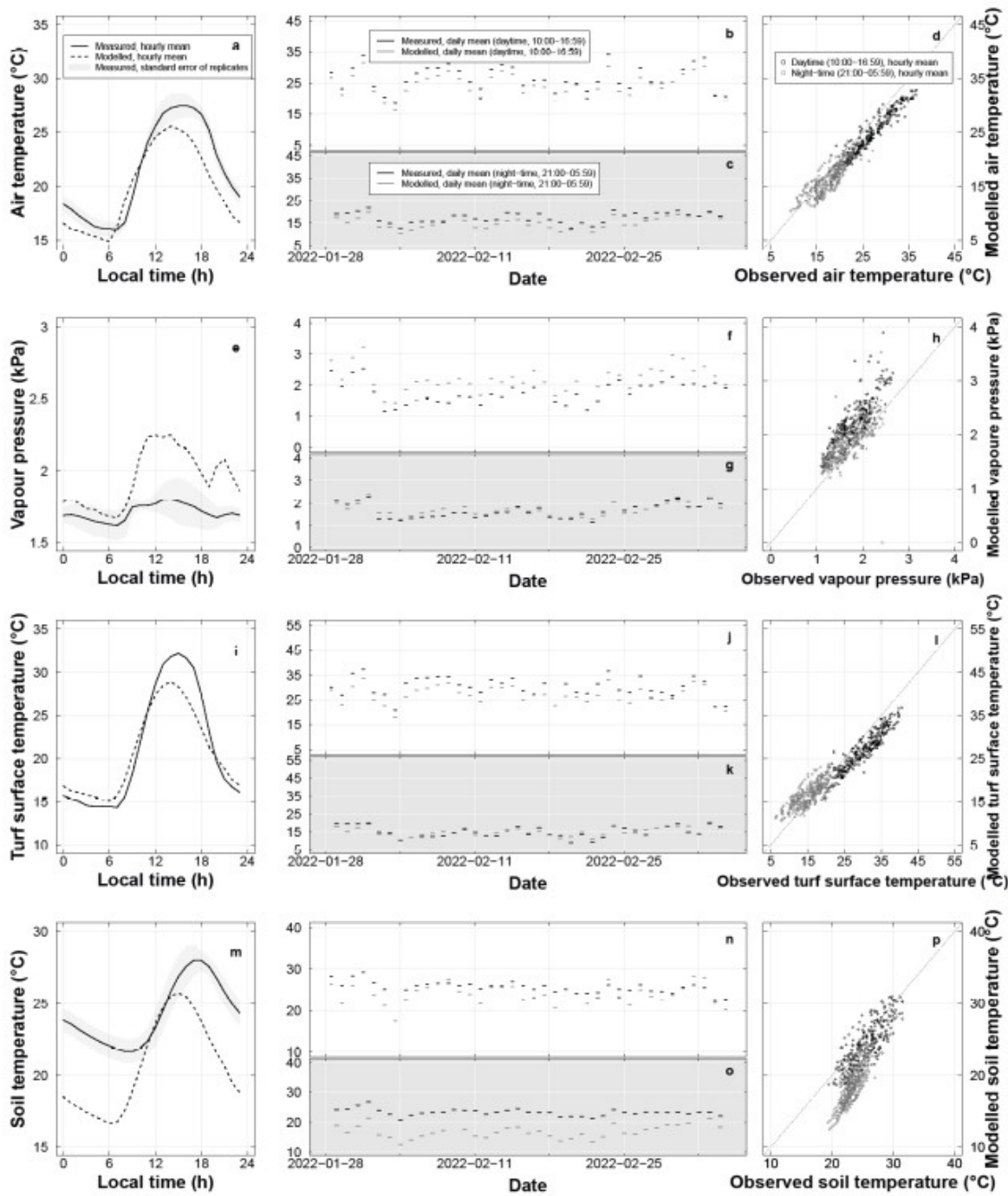


Fig. S11. Model evaluation that compared the modelled and the measured (a–d) air temperature, (e–h) vapour pressure (i–l) turf surface temperature, (m–p) soil temperature of the unirrigated scenario (plot). The modelled and measured data were compared in terms of their average diurnal cycles (left column),

daytime and night-time daily means (middle column) and scatter plot of hourly means (right column). In the middle column, the broken lines were a time series split into daytime (10:00–16:59, white panels) and night-time (21:00–05:59, grey panels). The model evaluation period was from 2022-01-28 to 2022-03-06.

Table S1

Urban Geometry, radiation, and conductive heat flux parameters used for simulation.

Parameter	Description	Unit	Value	Reference
H_{can}	Average height of urban canyon	m	5	Site condition
W_{can}	Ground width of urban canyon	m	50	Site condition
W_{roof}	Roof width of urban canyon	m	5	Site condition
N_{tree}	Absence (0) or presence (1) of trees	—	0	Site condition
$f_{r,\text{imp}}$	Fraction of impervious roof	—	0	Site condition
$f_{r,\text{veg}}$	Fraction of vegetated roof	—	0	Site condition
$f_{g,\text{imp}}$	Fraction of impervious ground	—	1	Site condition
$f_{g,\text{bare}}$	Fraction of bare ground	—	0	Site condition
$f_{g,\text{veg}}$	Fraction of vegetated ground	—	1	Site condition
α_r	Albedo roof [imp, veg]	—	[0.15,—]	(Nice et al., 2018)
α_g	Albedo ground [imp, bare, veg]	—	[—,0.22]	Measured
α_w	Albedo wall	—	0.3	(Nice et al., 2018)
ε_r	Emissivity roof [imp, veg]	—	[0.92,—]	(Nice et al., 2018) (Harshan et al., 2018)
ε_g	Emissivity ground [imp, bare, veg]	—	[—,0.97]	2018)
ε_w	Emissivity wall	—	[0.88]	(Nice et al., 2018)
$\lambda_{r,\text{imp}}$	Thermal conductivity of impervious roof	$\text{W K}^{-1} \text{m}^{-1}$	0.773	(Meili et al. 2020)
λ_w	Thermal conductivity of wall	$\text{W K}^{-1} \text{m}^{-1}$	0.342	(Meili et al. 2020)
$CV_{r,\text{imp}}$	Volmetric heat capacity of imprevious roof	$\text{MJ K}^{-1} \text{m}^{-3}$	0.813	(Meili et al. 2020)
CV_w	Volmetric heat capacity of wall	$\text{MJ K}^{-1} \text{m}^{-3}$	0.9035	(Meili et al. 2020)
dZ_r	Thickness of roof layers [1, 2]	m	[0.057, 0.057]	(Meili et al. 2020)
dZ_w	Thickness of wall layers [1, 2]	m	[0.074, 0.074]	(Meili et al. 2020)

Table S2

Vegetation parameters used for the simulation. Separate parameters for roof vegetation [r_{veg}], ground vegetation [g_{veg}], and trees [$tree$] are specified in this order.

Parameter	Description	Unit/code	Value [$r_{veg}, g_{veg}, tree$]	Reference
h_c	Ground vegetation canopy height	m	[-, 0.1, -]	Site condition
d_{leaf}	Leaf dimension	cm	[-, 2, -]	(Fatichi and Pappas, 2017)
LAI	Leaf area index	-	[-, 3, -]	(Fatichi and Pappas, 2017)
SAI	Stem area index	-	[-, 0.001, -]	(Fatichi and Pappas, 2017)
S_{LAI}	Specific leaf area	$m^2 \text{ LAI } g^{-1}$	[-, 0.016, -]	(Fatichi and Pappas, 2017)
K_{opt}	Canopy light extinction coefficient	-	[-, 0.5, -]	(Fatichi and Pappas, 2017)
VCASE _{root}	Vertical root profile (1, 2, 3, 4)	-	[-, 1, -]	(Fatichi and Pappas, 2017)
ZR ₉₅	Root depth, 95th percentile of vegetation	$\text{mm } m \text{ root } m^{-2}$	[-, 250, -]	Tested
RI _{root}	Root length index	PFT	[-, 4500, -]	(Fatichi and Pappas, 2017)
ψ_{Sto00}	Soil water potential at the beginning of stomatal closure	MPa	[-, -0.6, -]	(Fatichi and Pappas, 2017)
ψ_{Sto50}	Soil water potential at 50% stomatal closure	MPa	[-, -2, -]	(Fatichi and Pappas, 2017)
ψ_{L50}	Water potential at 50% leaf hydraulic conductivity	MPa	[-, -2.5, -]	(Fatichi and Pappas, 2017)
ψ_{X50}	Water potential at 50% of xylem hydraulic conductivity and limite for water extraction from soil	MPa	[-, -0.95, -]	(Fatichi and Pappas, 2017)
ϕ_p	Photosynthesis pathway	3:C3, 4:C4, or 5:CAM	[-, 3, -]	(Fatichi and Pappas, 2017)
K_N	Canopy nitrogen decay coefficient	-	[-, 0.3, -]	(Fatichi and Pappas, 2017)
$V_{c,max}$	Maximum Rubisco capacity at 25°C leaf scale	$\mu\text{mol CO}_2 \text{ m}^{-2} \text{ s}^{-1}$	[-, 64, -]	Tested
g_{0,CO_2}	Minimum/cuticular stomatal conductance	$\text{mol CO}_2 \text{ m}^{-2} \text{ leaf s}^{-1}$	[-, 0.01, -]	(Fatichi and Pappas, 2017)
a_1	Empirical parameter linking net assimilation AnC to stomatal conductance g_{s,CO_2}	- $\mu\text{mol equivalent CO}_2 \text{ mol CO}_2 \text{ photon}^{-1}$	[-, 7, -]	(Fatichi and Pappas, 2017)
r_{jv}	Scaling factor between J_{max} and $V_{c,max}$	$\mu\text{mol CO}_2 \text{ Pa}^{-1}$	[-, 2.1, -]	(Fatichi and Pappas, 2017)
ϵ_{FI}	Intrinsic quantum efficiency	-	[-, 0.081, -]	(Fatichi and Pappas, 2017)
$\Delta_{0,r}$	Empirical coefficient that expresses the value of vapour pressure deficit at which $f(\Delta e) = 0.5$	Pa	[-, 2000, -]	Tested

Table S3

Soil, interception, and runoff parameters used for the simulation.

Parameter	Description	Unit/code	Value/code	Reference
$Z_{s,g}$	Ground soil layer discretisation	mm	[0 … 2000]	(Meili et al., 2020)
$F_{g,soil}$	Ground soil composition [f_{clay} , f_{sand} , $f_{organic}$]	—	[0.2, 0.4, 0.06]	Tested (Meili et al., 2020)
K_{imp}	Hydraulic conductivity of impervious surface [roof, ground]	mm h ⁻¹	[0, —]	(Meili et al., 2020)
K_{bot}	Hydraulic conductivity at the bottom of the last soil layer [roof, ground]	mm h ⁻¹	[—, free drainage]	(Meili et al., 2020)
SPAR	Soil parameter type [roof, ground]	1: VanGenuchten or 2: Saxton–Rawls	[, 2]	(Meili et al., 2020)
In_{imp}^{max}	Maximum interception capacity of impervious surfaces [roof, ground]	mm	[0.25, 0.5]	(Meili et al., 2020)
In_{soil}^{max}	Maximum interception capacity on top of soil [r,veg, g,bare, g,veg]	mm	[—, —, 10]	(Meili et al., 2020)
$S_{p,in}^{max}$	Specific water retained by vegetation surface [r,veg, g,bare, g,veg]	mm m ² PFT area	[—, —, 0.1]	(Meili et al., 2020)
λ_r	Percentage of runoff that leaves the system [roof, ground]	m ⁻² leaf area	[1, 0.5]	(Meili et al., 2020)
Z_{ifc}	Depth from which initial soil moisture content is at field capacity	mm	100	Tested
Z_{fc}	Depth from which soil moisture content is at field capacity	mm	400	Tested

Table S4

Location and measurement parameters, and anthropogenic heat used for the simulation.

Parameter	Description	Unit	Value	Reference
ϕ_{data}	Latitude (positive north)	°	-37.83	Site condition
λ_{data}	Longitude (positive east)	°	145.02	Site condition
θ_{canyon}	Canyon orientation [direction 1, direction 2] Difference between local time and Greenwich	°	25	Site condition
Δ_{GMT}	Meridian Time	h	10	Site condition
Z_{atm}	Atmospheric forcing/reference height	m	80	Data (Meili et al., 2020)
$T_{\text{b,min}}$	Minimum interior building temperature	°C	18	(Meili et al., 2020)
$T_{\text{b,max}}$	Maximum interior building temperature	°C	27	(Meili et al., 2020)
$Q_{\text{f,roof}}$	Anthropogenic heat input on top of roof	W m^{-1}	0	Site condition
$Q_{\text{f,can}}$	Anthropogenic heat input within canyon	W m^{-1}	0	Site condition

Table S5

Root mean square errors of modelled air temperature difference between the irrigated and unirrigated scenarios for six model parameters at four different levels. These six parameters are site-specific and therefore a testing is conducted to find out the level that generates the lowest root mean square error or is most representative of the site conditions based on our local knowledge using 2021's data. The chosen level for subsequent simulations is in bold.

Depth below which initial soil moisture is at field capacity (mm)	0	100	200	400
Root mean square error (°C)	0.490	0.515	0.601	0.837
Depth below which soil moisture is kept at field capacity (mm)	100	200	400	800
Root mean square error (°C)	0.459	0.493	0.489	0.515
Ground soil composition [f_{clay} , f_{sand} , f_{organic}]	0.2, 0.4, 0.025	0.2, 0.4, 0.06	0.05, 0.75, 0.06	0.1, 0.7, 0.06
Root mean square error (°C)	0.489	0.558	1.095	1.102
Empirical coefficient that expresses the value of vapour pressure deficit at which $f(\Delta e) = 0.5$ (Pa)	500	1000	2000	4000
Root mean square error (°C)	0.549	0.489	0.452	0.461
Root depth, 95th percentile of vegetation (mm)	250	300	350	400
Root mean square error (°C)	0.452	0.457	0.456	0.455
Maximum Rubisco capacity at 25°C leaf scale ($\mu\text{mol CO}_2 \text{ m}^{-2} \text{ s}^{-1}$)	54	64	74	84
Root mean square error (°C)	0.452	0.456	0.533	0.474

References of supplementary materials

- Fatichi, S., Pappas, C., 2017. Constrained variability of modeled T : ET ratio across biomes. *Geophys. Res. Lett.* 44, 6795–6803. <https://doi.org/10.1002/2017GL074041>
- Harshan, S., Roth, M., Velasco, E., Demuzere, M., 2018. Evaluation of an urban land surface scheme over a tropical suburban neighborhood. *Theor. Appl. Climatol.* 133, 867–886.
<https://doi.org/10.1007/s00704-017-2221-7>
- Meili, N., Manoli, G., Burlando, P., Bou-Zeid, E., Chow, W.T.L., Coutts, A.M., Daly, E., Nice, K.A., Roth, M., Tapper, N.J., Velasco, E., Vivoni, E.R., Fatichi, S., 2020. An urban ecohydrological model to quantify the effect of vegetation on urban climate and hydrology (UT&C v1.0). *Geosci. Model Dev.* 13, 335–362. <https://doi.org/10.5194/gmd-13-335-2020>
- Nice, K.A., Coutts, A.M., Tapper, N.J., 2018. Development of the VTUF-3D v1.0 urban micro-climate model to support assessment of urban vegetation influences on human thermal comfort. *Urban Clim.* 24, 1052–1076. <https://doi.org/10.1016/j.uclim.2017.12.008>